Research on Sliding Wear of Angular Contact Ball Bearing Raceway Under Combined Load

Xiang Liu , Chuan Zhao , Fangchao Xu * , Wenhui Zhao , Junjie Jin , Rui Man , Jichao Liu , Feng Sun *

Posted Date: 23 April 2026

doi: 10.20944/preprints202604.1721.v1

Keywords: rolling bearing; joint load; wear model; numerical calculation

 doi:10.20944/preprints202604.1721.v1

Article

Research on Sliding Wear of Angular Contact Ball Bearing Raceway Under Combined Load

Xiang Liu [1], Chuan Zhao [1], Fangchao Xu [1,*], Wenhui Zhao [1], Junjie Jin [1], Rui Man [1,2], Jichao Liu [2] and Feng Sun [1,*]

[1] School of Mechanical Engineering, Shenyang University of Technology, Shenyang 110870, China

[2] General Technology Group Machine Tool Engineering Research Institute Co., Ltd., 4 Wangjing Road, Beijing 100102, China

* Correspondence: xufangchao@sut.edu.cn (F.X.); sunfeng@sut.edu.cn (F.S.)

Abstract

Based on outer raceway control theory and considering the effects of elastic deformation, centrifugal force, and gyroscopic moment between the rolling elements and raceways, a geometric and force analysis of angular contact ball bearings is conducted. A five-degree-of-freedom theoretical model capable of accounting for the combined action of radial force and moment is established. The accuracy of the model is verified through numerical calculations and experimental results from existing literature. Upon validation of the theoretical model, a modified Archard model is employed to develop a wear volume model for the bearing raceways. The influence of both single and combined loads on sliding wear in the bearing raceways is systematically analyzed.

Keywords: rolling bearing; joint load; wear model; numerical calculation

1. Introduction

Angular contact ball bearings (ACBBs) are critical components in precision rotating machinery. Under combined loads, the dynamic parameters of the raceway exhibit complex nonlinear behavior, which influences slow sliding wear during long-term operation.

Jones[1] first proposed a theoretical model for ACBB analysis and introduced raceway control modes for low- and high-speed conditions. Harris[2] analytically investigated the effects of axial force and rotational speed on the dynamic parameters of precision bearings. DE et al.[3] developed a pseudo-static model for ACBBs and studied their dynamic parameters analytically, though without considering gyroscopic moments on the rolling elements. Jiang, Guo et al.[4,5] incorporated gyroscopic moments and preload into quasi-static models to analyze bearing dynamics. Based on force equilibrium, Gunduz et al.[6] derived a theoretical model for typical bearing mounting configurations and compared the effects of axial load on dynamic behavior. Wang et al.[7] investigated the influence of speed and radial force variations on dynamic parameters. He et al.[8] examined dynamic changes under pure axial load, accounting for centrifugal force and thermal expansion. Zhang et al.[9] validated a pseudo-static method for ACBBs and studied the effect of load variation on raceway dynamics.

In terms of wear modeling, EL-THALJI et al.[10] simulated the wear process in rolling bearings and correlated vibration characteristics with wear progression. ALFARES M A et al.[11] studied the influence of preload on wear rate and suggested optimal preload levels to minimize wear. LIU CH et al.[12] applied the Archard model to estimate wear life in ACBBs. Similar approaches were adopted by Olofsson, Janakiraman et al.[13,14] and Liu et al.[15]. Yang et al.[16,17] focused on the effect of torque on spindle bearing wear.

While extensive research has been conducted on the theory and wear dynamics of ACBBs, most studies on dynamic parameters and wear have considered limited load conditions, such as single axial, radial, or torque loads, or combinations of two, which do not fully represent complex multi-

 doi:10.20944/preprints202604.1721.v1

axis loading scenarios in practical applications. Moreover, few investigations have addressed raceway wear-related dynamic parameters under combined loads, despite their critical importance for bearing reliability and lifespan. In this paper, a theoretical model and wear dynamics model for ACBBs are developed to examine the variation in dynamic parameters and raceway wear under combined loading conditions, providing insights for more accurate life prediction and maintenance strategies.

2. Theoretical Model of Angular Contact Ball Bearing

2.1. Geometric Analysis

Figure 1 shows the static state geometric structure of the bearing. the center of the ball O_b is in the same straight line as the inner curvature centers O_i and outer curvature centers O_o. The inner and outer contact angles α_i, α_o are the same with the initial contact angles α_0. The distance between O_i and O_o is BD, and the component of the distance between O_i the bearing center in the radial plane is R_i.

$$BD = (f_i + f_o - 1)D_b \tag{1}$$

$$R_i = 0.5d_m + (f_i - 0.5)D_b \cos\alpha_0 \tag{2}$$

The inner curvature radius coefficient is $f_i = r_i / D_b$, the inner curvature radius is r_i; the outer curvature radius coefficient is $f_o = r_o / D_b$, the outer curvature radius is r_o; the ball's diameter is D_b, the pitch circle diameter is d_m, $\gamma = D_b / d_m$.

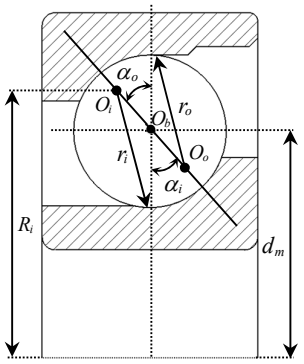

Figure 1. Angular contact ball bearing geometry.

Under combined load and speed, displacement vector between inner and outer ring is $\delta_b = [\delta_x\ \delta_y\ \delta_z\ \theta_x\ \theta_y]$, δ_x, δ_y are radial displacement perpendicular to each other, δ_z is axial displacement, and θ_x and θ_x are inclination angles generated by X, Y axes. in Figure 2, φ_j is the j-th ball's position angle along the raceway, and the ball's number is Z, then $\varphi_j = 2\pi(j-1)/Z$.

 doi:10.20944/preprints202604.1721.v1

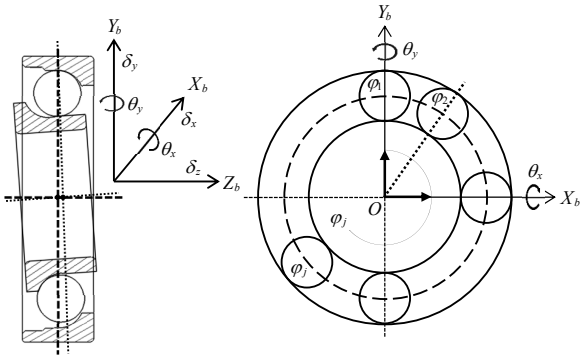

Figure 2. Radial and axial view of the bearing.

Under high speed, affected by centrifugal and gyroscopic effects, causing ball at each azimuth angle to deviate from the geometric position in the static state. O_i , O_b and O_o change from three points and one line in the static state to the broken line state as shown in Figure 3. Under most working conditions, outer ring does not rotate in system, so O_o is unchanged.

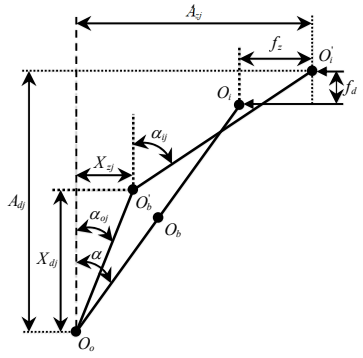

Figure 3. The relationship between ball and raceway.

In Figure 3, f_d is the radial component of the motion from O_i to O_i' and the axial component is f_z . Under the influence of elastic deformation. The distance between the ball's center to the inner and outer raceway's center becomes $\overline{O_b'O_i'}$, $\overline{O_b'O_o}$. The radial and axial distance from O_i to O_o becomes A_{dj} , A_{zj} ; The inner, outer contact angle becomes α_{ij} and α_{oj} ; The radial and axial distances from O_b to O_i , O_o becomes X_{dj} , X_{zj} .

$$f_d = \delta_x \sin\varphi_j + \delta_y \cos\varphi_j \, , \, f_z = \delta_z + R_i(\theta_x \cos\varphi_j - \theta_y \sin\varphi_j) \tag{3}$$

$$\overline{O_b'O_i'} = (f_i - 0.5)\cdot D_b + \delta_{ij} \, , \, \overline{O_b'O_o} = (f_o - 0.5)\cdot D_b + \delta_{oj} \tag{4}$$

$$A_{dj} = BD\cos\alpha_0 + f_d \, , \, A_{dj} = \overline{O_b'O_o}\cos\alpha_{oj} + \overline{O_b'O_i'}\cos\alpha_{ij} \tag{5}$$

$$A_{zj} = BD\sin\alpha_0 + f_z \, , \, A_{zj} = \overline{O_b'O_o}\sin\alpha_{oj} + \overline{O_b'O_i'}\sin\alpha_{ij} \tag{6}$$

$$\cos\alpha_{ij} = \frac{A_{dj} - X_{dj}}{\overline{O_b'O_i'}} \, , \, \sin\alpha_{ij} = \frac{A_{zj} - X_{zj}}{\overline{O_b'O_i'}} \, , \, \cos\alpha_{oj} = \frac{X_{dj}}{\overline{O_b'O_i'}} \, , \, \sin\alpha_{oj} = \frac{X_{zj}}{\overline{O_b'O_i'}} \tag{7}$$

According to the geometric relation of the ball's center O_b' in Figure 3, the displacement coordination equation of the j -th ball can be obtained as

 doi:10.20944/preprints202604.1721.v1

$$(A_{dj} - X_{dj})^2 + (A_{zj} - X_{zj})^2 = \overline{O_b' O_i'^2},\ X_{dj}^{\ 2} + X_{zj}^{\ 2} = \overline{O_b' O_o'^2} \tag{8}$$

2.2. Force Analysis of Angular Contact Ball Bearing

Figure 4 shows the ball's state under stress, F_{cj} is the ball's centrifugal force, M_{gj} is the gyro moment generated by the constant change of the rolling body rotation axis. Q_{ij}, Q_{oj} is the normal force acting on the ball. F_{ij} and F_{oj} are respectively the ball's surface friction caused by inner and outer raceway, which is used to balance the gyro-torque generated by the ball.

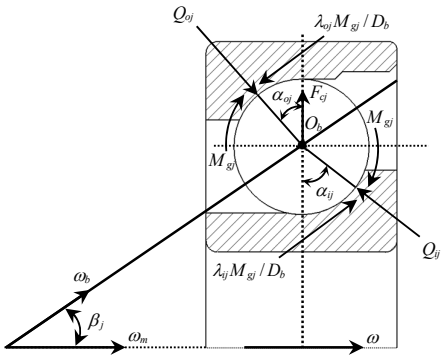

Figure 4. Force analysis of the ball.

$$F_{cj} = \frac{1}{2} m d_m \omega^2 \left(\frac{\omega_m}{\omega}\right)_j^2 \tag{9}$$

$$M_{gj} = J\omega^2 \sin\beta \left(\frac{\omega_b}{\omega}\right)_j \left(\frac{\omega_m}{\omega}\right)_j \tag{10}$$

$$Q_{ij} = K_{ij}\delta_{ij}^{3/2},\ Q_{oj} = K_{oj}\delta_{oj}^{3/2} \tag{11}$$

$$F_{ij} = \frac{2(1-\lambda_j)M_{gj}}{D_b},\ F_{oj} = \frac{2\lambda_j M_{gj}}{D_b} \tag{12}$$

In formula (9), the ball's mass is m, and ω_m / ω is the ratio of the ball's revolution velocity to the inner ring's velocity, which can be calculated according to Formula (13). In formula (10), $J = \rho\pi D_b^5 / 60$ is the ball's rotational inertia; The ball's density is ρ; The ball's attitude angle is β, which can be calculated according to formula (14); ω_b / ω is the ratio of the ball's rotation velocity to the inner ring's velocity, which can be calculated according to Formula (15). In formula (11), K_{ij}, K_{oj} is the contact stiffness between ball and inner, outer rings, the calculation method in reference [18] can be referred to. The value of λ_j in equation (12) is determined by the raceway integrated control method in literature [2].

$$\left(\frac{\omega_m}{\omega}\right)_j = \frac{1-\gamma\cos\alpha_{ij}}{1+\cos(\alpha_{ij}-\alpha_{oj})} \tag{13}$$

$$\beta = \arctan\frac{\sin\alpha_o}{\cos\alpha_o + \gamma} \tag{14}$$

 doi:10.20944/preprints202604.1721.v1

$$\left(\frac{\omega_b}{\omega}\right)_j = \frac{-1}{(C_{oj}+C_{ij})\gamma\cos\beta_j} \tag{15}$$

$$C_{oj} = \frac{\cos\alpha_{oj}+\tan\beta_j\sin\alpha_{oj}}{1+\gamma\cos\alpha_{oj}}, C_{ij} = \frac{\cos\alpha_{ij}+\tan\beta_j\sin\alpha_{ij}}{1-\gamma\cos\alpha_{ij}} \tag{16}$$

When the forces acting on the ball reach equilibrium in the axial and radial directions, the ball's force equation are

$$\begin{cases} Q_{ij}\sin\alpha_{ij} - F_{oj}\cos\alpha_{ij}/2 = Q_{oj}\sin\alpha_{oj} - F_{oj}\cos\alpha_{oj}/2 \\ Q_{ij}\cos\alpha_{ij} + F_{oj}\cos\alpha_{ij}/2 + F_{cj} = Q_{oj}\cos\alpha_{oj} + F_{oj}\sin\alpha_{oj}/2 \end{cases} \tag{17}$$

The inner ring is balanced under axial, radial and torque loads, then the bearing five degrees of freedom force balance equation is

$$\begin{cases} F_x = \sum_{j=1}^{z}(Q_{ij}\cos\alpha_{ij} + F_{oj}\sin\alpha_{ij}/2)\sin\varphi_j \\ F_y = \sum_{j=1}^{z}(Q_{ij}\cos\alpha_{ij} + F_{oj}\sin\alpha_{ij}/2)\cos\varphi_j \\ F_z = \sum_{j=1}^{z}(Q_{ij}\sin\alpha_{ij} - F_{oj}\cos\alpha_{ij}/2) \end{cases} \tag{18}$$

$$\begin{cases} M_x = \sum_{j=1}^{z}\left((Q_{ij}\sin\alpha_{ij} - F_{oj}\cos\alpha_{ij}/2)R_i\cos\varphi_j + F_{oj}r_i\cos\varphi_j\right) \\ M_y = \sum_{j=1}^{z} -\left((Q_{ij}\sin\alpha_{ij} - F_{oj}\cos\alpha_{ij}/2)R_i\sin\varphi_j + F_{oj}r_i\sin\varphi_j\right) \end{cases} \tag{19}$$

2.3. Theoretical Model Solving and Verification

To test the accuracy of the numerical calculation, the rotational angular velocity ω_b, rotational angular velocity ω_m, contact Angle α_i and α_o, contact load Q_i and Q_o and rolling ratio of the ball were solved by specified working conditions, the solution results of each parameter is compared with literature [19]. The design parameters of the bearings used for numerical verification are shown in Table 1, and their working parameters are $F_{x/y} = 0N$, $M_{x/y} = 0N\cdot m$, $F_z = 889.84N$, $\omega = 15000r/\min$. Table 2 shows the calculation results and errors of bearing parameters.

Table 1. The design parameter of the bearing.

D_b	α_0	Z	$r_{i/o}$	d_m
15.081mm	25°	19	7.8421mm	105mm

Table 2. The verification of the dynamic parameter solution.

Dynamic parameter	Literature result	Results of this paper	error
$\omega_b/(r/\min)$	57670	57716	0.079%
$\omega_m/(r/\min)$	7255	7251	-0.055%
$\alpha_i/(^\circ)$	37.7	37.6	-0.27%
$\alpha_o/(^\circ)$	4.074	4.070	-0.098%
$Q_i/(N)$	76.57	76.73	0.21%
$Q_o/(N)$	488.97	490.76	0.37%
Spin-to-roll ratio	0.689	0.687	-0.29%

 doi:10.20944/preprints202604.1721.v1

According to the calculation results in Table 2, the parameters representing the contact, movement and force are very similar with literature [19], and the maximum error is less than 0.4%, which proves the accuracy of the theoretical model.

3. Sliding Wear Model of Angular Contact Ball Bearing Raceway

3.1. Raceway Wear Volume Model

Considering the non-uniform distribution of sliding speed and stress in inner and outer raceway's contact ellipse. Based on Archard original expression $V = KFL$, the tiny contact area within the contact ellipse dA is defined as the wear surface, dF is the contact pressure acting on dA. The micro sliding distance on dA is dL; Then the small wear volume dV on dA is

$$dV = kdFdL \tag{20}$$

where k stands for wear coefficient; $dF = pdA$, p stands for contact stress; $dL = vdt$, v stands for sliding speed, and dt is the sliding time. The calculation model of raceway wear volume of bearing shows as equation 21.

$$V = \int dV = \iint kpvdAdt \tag{21}$$

3.1.1. Calculation and Analysis of Wear Coefficient

Considering the material hardness, the expression for k is

$$k = (\alpha^* \times \Lambda^{\beta^*}) / H \tag{22}$$

where, α^* and β^* are the characteristic parameters of the contact auxiliary material and lubricant; H is Brinell hardness of bearing material; $\Lambda = h_{\min} / \sqrt{\sigma_r^2 + \sigma_g^2}$ is the oil film parameter, $h_{\min}$ stands for minimum film thickness, σ_r, σ_b stands for the surface roughness parameters, where $h_{\min}$ can be expressed as

$$h_{\min} = 3.63U^{0.68}G^{0.49}W^{-0.073}(1-e^{-0.68\kappa})R_x \tag{23}$$

$G = \xi E$ stands for viscosity parameter, ξ stands for oil film pressure parameters, E stands for effective elastic modulus. $W = Q_{i/j} / (R_x)^2 E$ is the dimensionless load parameter, R_x and R_y are the contact ellipse equivalent radii. $e = \sqrt{1-(b/a)^2}$ is the eccentricity of the ellipse, a, b are the contact ellipse's major and minor axes. $\kappa = 1.0339(R_y / R_x)^{0.636}$ is the ellipticity parameter; $U = \eta_0 u / ER_x$ is the dimensionless speed parameter, η_0 is lubricating oil viscosity parameter, and u stands for rolling speed in raceway contact ellipse. The expressions of the internal and outer raceway parameters R_x, R_y and u are

$$\begin{cases} R_{xij} = (D_b / 2)(1 - D_b \cos\alpha_{ij} / d_m) \\ R_{yi} = D_b f_i / (2f_i - 1) \\ u_{ij} = (\omega - \omega_{mj})(d_m - D_b \cos\alpha_{ij}) / 2 \end{cases} \tag{24}$$

$$\begin{cases} R_{xoj} = (D_b / 2)(1 + D_b \cos\alpha_{oj} / d_m) \\ R_{yo} = D_b f_o / (2f_o - 1) \\ u_{oj} = -\omega_{mj}(d_m + D_b \cos\alpha_{oj}) / 2 \end{cases} \tag{25}$$

 doi:10.20944/preprints202604.1721.v1

The material parameters α^* and β^* involved in the formula are 3.433×10^{-8} and -1.032 respectively; H takes 8470Mpa; σ_r and σ_b take 0.18μm; ξ takes 2.2×10^{-8}m^2/N; η_0 takes 0.04pa·s; E takes 1.12×10^{5}Mpa.

This paper explores the variation law of wear coefficient under the action of speed, radial force, moment, combined load. The influence law of speed is shown in Figure 5, the influence law of unilateral radial force and unilateral moment is shown in Figure 6 and 7, and the influence law of combined load is shown in Figure 8, 9, 10.

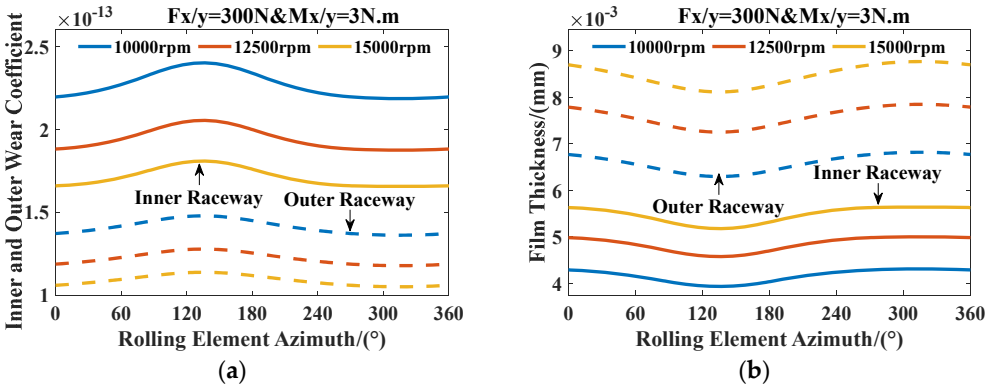

Figure 5. Effect of speed on wear coefficient and Film.

As shown in Figure 5, when radial force $F_{x/y} = 300N$ and torque $M_{x/y} = 3N \cdot m$ remain unchanged, k_i and k_o are negatively correlated with speed, while $h_{\min i/o}$ is positively correlated with speed, The different changes of wear coefficient and oil film thickness indicate that the oil film thickness of raceway increases with the increase of speed, and the formation of oil film and the increase of thickness reduce the wear coefficient.

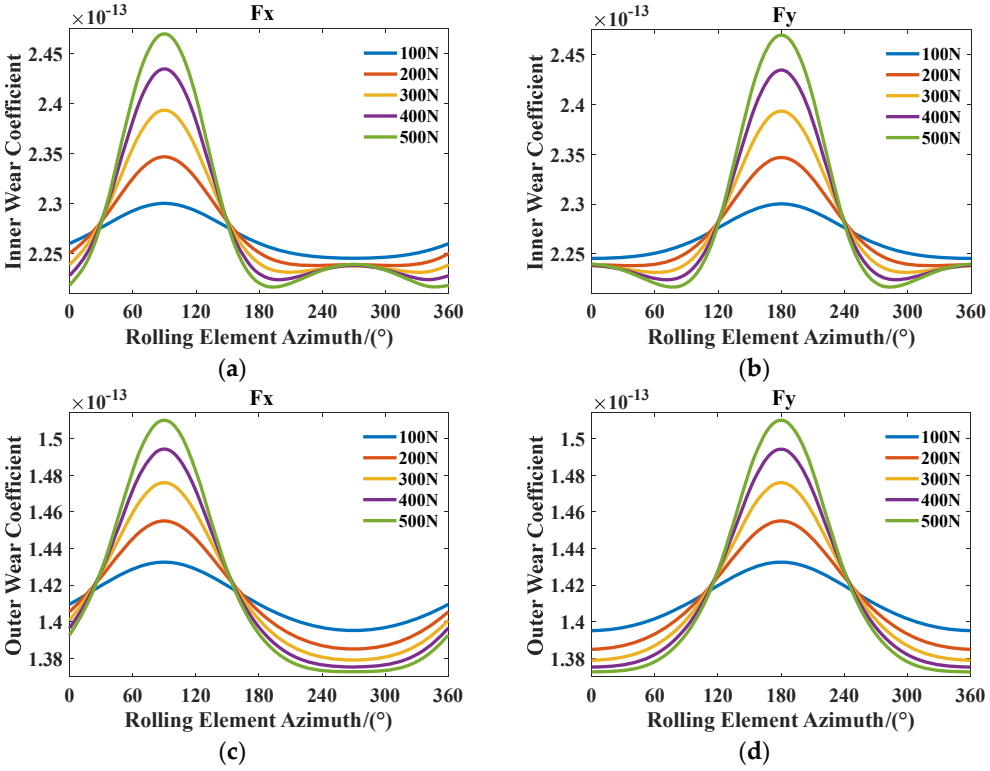

Figure 6. Effect of unilateral radial force on wear coefficient.

 doi:10.20944/preprints202604.1721.v1

As shown in Figure 6, in the bearing zone, k_i and k_o is positively correlated with the radial force F_x and F_y, and reaches the maximum value in radial force direction. In the non-bearing zone, k_o is negatively correlated with F_x and F_y, while k_i presents a W-shaped variation rule, and becomes obvious gradually with the increase of F_x.

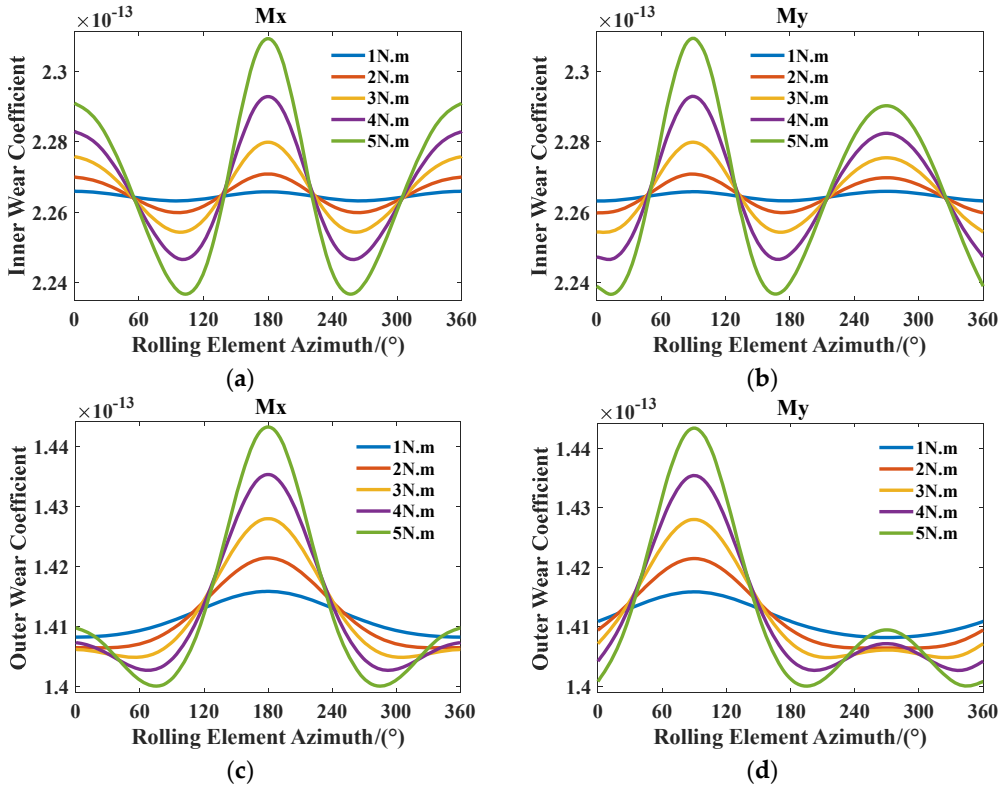

Figure 7. Effect of unilateral torque on wear coefficient.

As shown in Figure 7. Under the action of torque, the inner raceway has two bearing zones. When M_x acts, the azimuth near 0°and 180°is the bearing zone; when M_y acts, the azimuth near 90°and 270°is the bearing zone. In the bearing area, the wear coefficient of raceway inside and outside is positively correlated with M_x and M_y. In the non-bearing zone, k_i is negatively correlated with M_x and M_y, while k_o presents a W-shaped variation rule, and gradually becomes obvious with the increase of torque.

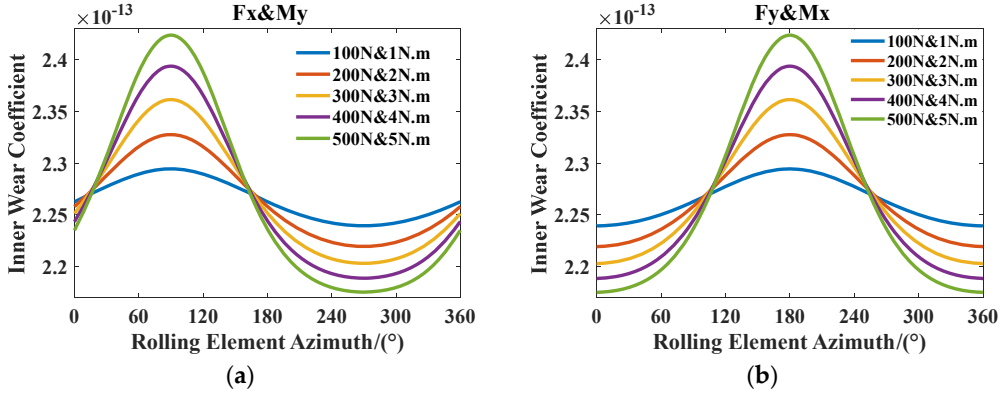

 doi:10.20944/preprints202604.1721.v1

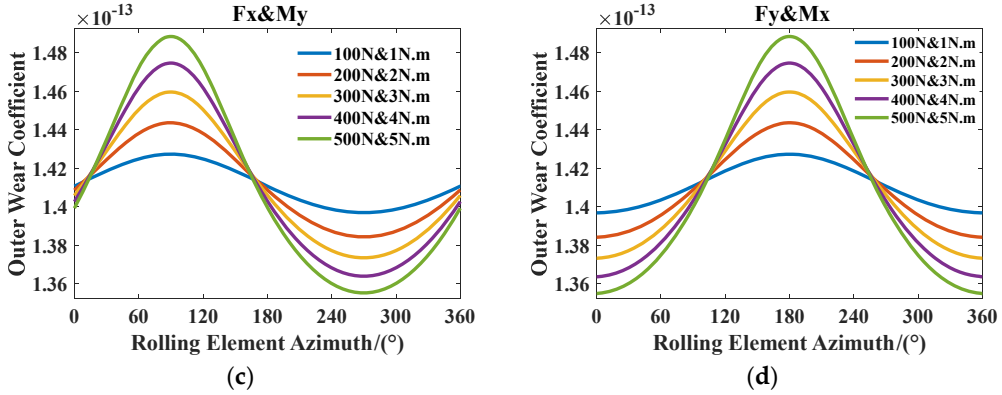

Figure 8. Effect of force and torque on wear coefficient.

As shown in Figure 8. The positive direction of the torque M_y is the same as the radial force F_x, and the positive direction of the M_x is the same as the radial force F_y. In the bearing area, k_i and k_o is positively correlated with the combined load. In the non-bearing area, k_i and k_o is negatively correlated with the combined load.

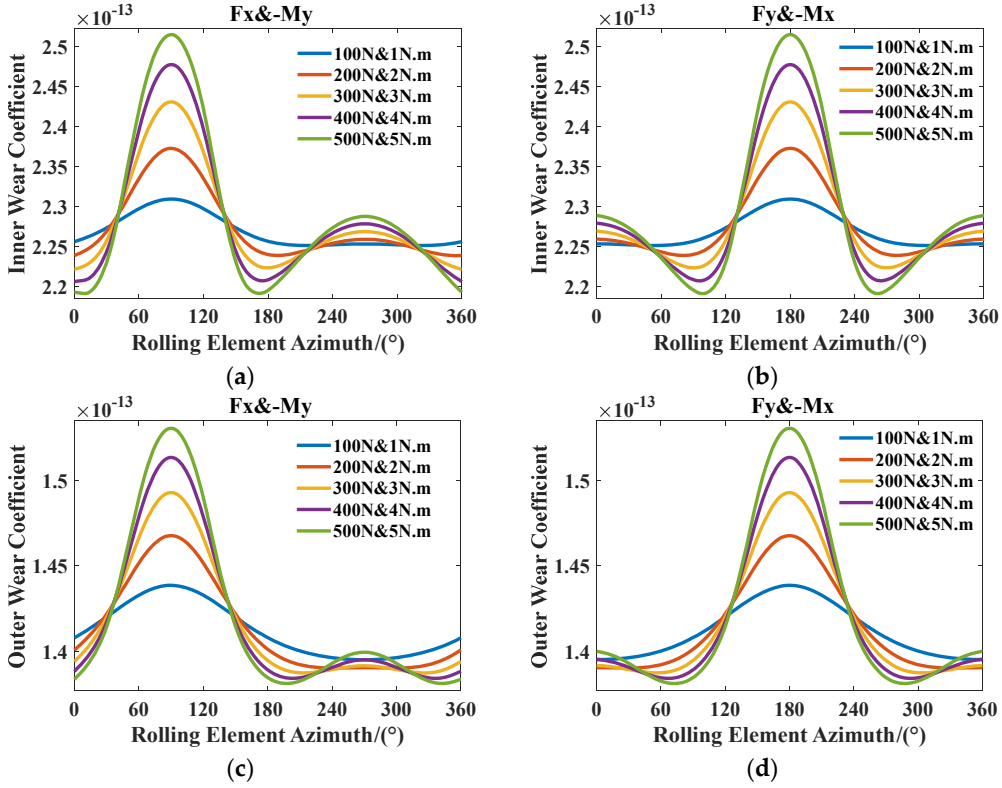

Figure 9. Effect of force and torque on wear coefficient.

As shown in Figure 9. The positive direction of the torque $-M_y$ is opposite to the radial force F_x, and the positive direction of the $-M_x$ is opposite to the radial force F_y. In the bearing area, the wear coefficient of raceway inside and outside is positively correlated with the combined load. In the non-load zone, k_i and k_o shows W-shaped change, among which the W-shaped phenomenon in inner raceway is much obvious than that in outer raceway, and the W-shaped change is gradually obvious with the increase of the combined load.

 doi:10.20944/preprints202604.1721.v1

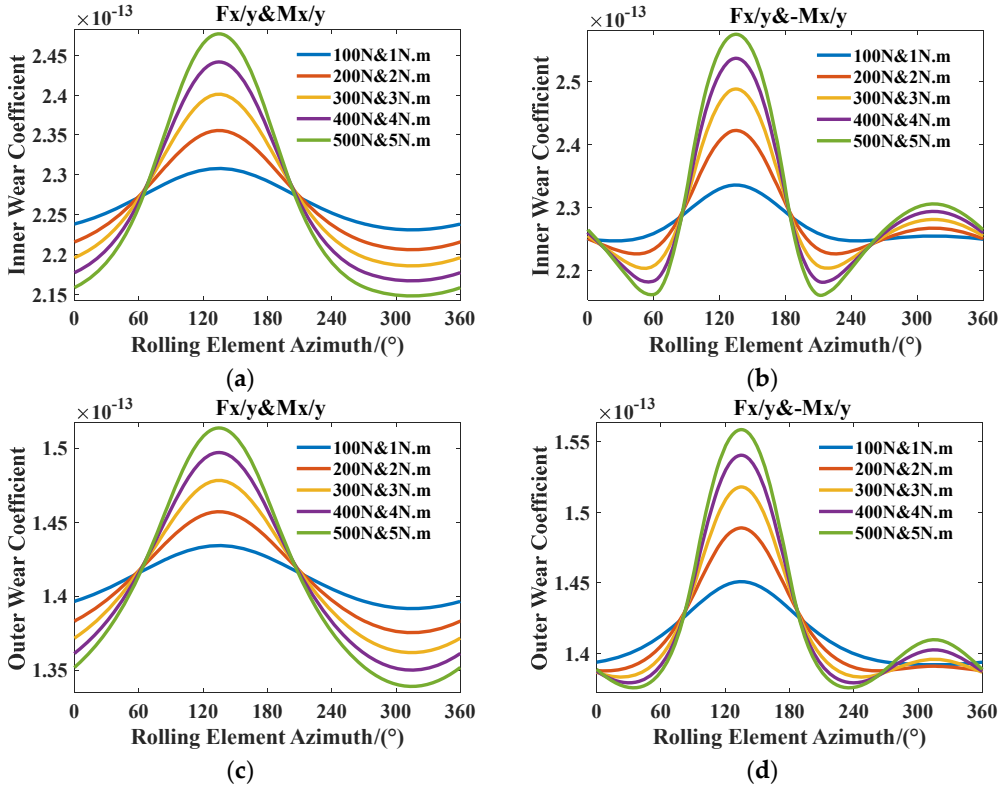

Figure 10. Effect of combined load on wear coefficient.

As shown in Figure 10. When the radial force and torque act in the same direction, k_i and k_o is positively correlated with the combined load in bearing zone, and negatively correlated with combined load in non-bearing zone. When torque and radial force act in the opposite direction, k_i and k_o is positively correlated with the combined load in the bearing zone, and presents a W-shaped change in the non-bearing zone. The W-shaped phenomenon of the inner raceway is more obvious than that of the outer raceway, and the W-shaped change is gradually obvious with the increase of the combined load.

3.1.2. Study on the Distribution of Sliding Velocity in a Contact Ellipse

As shown in Figure 11, the differential sliding velocity $v_{yi/o}$ at minor axis b and spin sliding velocity $\omega_{si/o}$ of the ball form the sliding velocity on the contact ellipse. The expressions for $v_{yi/o}$, $\omega_{si/o}$ and total sliding velocity $v(x,y)_{i/o}$ are shown in equations 26, 27and 28.

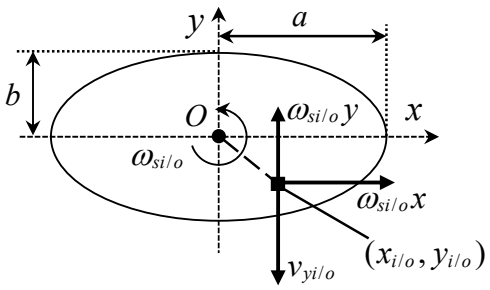

Figure 11. Sliding velocity distribution on contact ellipse.

 doi:10.20944/preprints202604.1721.v1

$$\begin{cases} v_{yi} = -\omega d_m / 2 - \left\{ (r_i^2 - x_i^2)^{1/2} - (r_i^2 - a_i^2)^{1/2} + [(D_b / 2)^2 - a_i^2]^{1/2} \right\} \times (\omega_b \sin\beta \sin\alpha_i - \omega \cos\alpha_i) \\ v_{yo} = \left\{ (r_o^2 - x_o^2)^{1/2} - (r_o^2 - a_o^2)^{1/2} + [(D_b / 2)^2 - a_o^2]^{1/2} \right\} \times (\omega_b \cos(\beta - \alpha_o)) \end{cases} \tag{26}$$

$$\begin{cases} \omega_{si} = \omega_b \sin(\beta - \alpha_i) + \omega \sin\alpha_i \\ \omega_{so} = \omega_b \sin(\alpha_o - \beta) \end{cases} \tag{27}$$

$$v(x, y)_{i/o} = [(v_{yi/o} - \omega_{si/o} y)^2 + (\omega_{si/o} x)^2]^{1/2} \tag{28}$$

Under the conditions of $F_x = F_y = 300N$, preload 500N, and rotational speed 10000r/min, the ball located at 135°is selected to calculate its total sliding velocity distribution on the contact ellipse. The calculation results is shown as Figure 12.

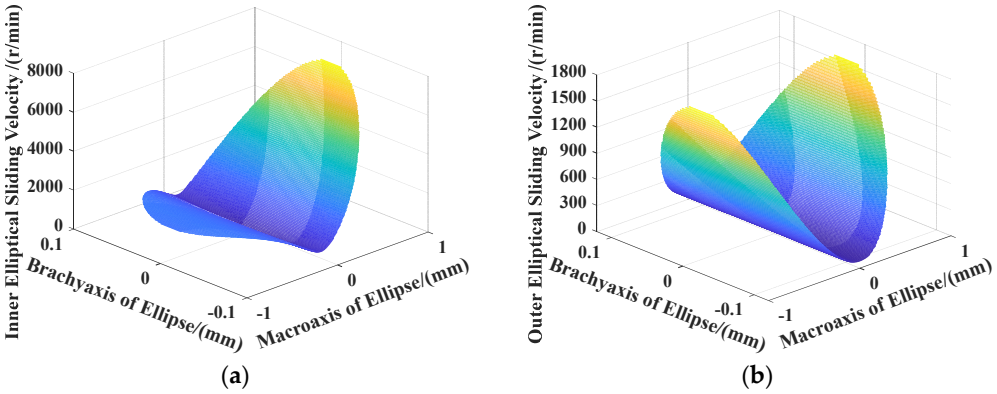

Figure 12. Sliding velocity distribution in contact ellipse.

As shown in Figure 12, the total sliding velocity remains stable along short axis and reaches a minimum in center. Along the long axis, the inner raceway's total sliding velocity presents an asymmetric distribution, while presents a symmetrical distribution on the outer raceway.

The sliding velocity at the center of the contact ellipse is studied in this paper, study condition are rotational speed, unilateral radial force, unilateral moment, and combined load, the influence law of rotational speed shows in Figure 13, the influence law of unilateral radial force and unilateral moment is shown in Figure 14 and 15, and the combined load's influence is shown in Figure 16, 17 and 18.

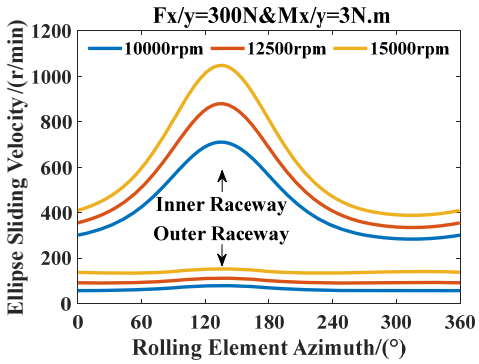

Figure 13. Effect of speed on sliding velocity at the center of raceway contact ellipse.

As shown in Figure 13, the raceway's sliding velocity is positively correlated with speed, and reaches a maximum value at the direction of the load, and the sliding velocity of the inner raceway and its variation with the speed are greater than that of the outer raceway.

 doi:10.20944/preprints202604.1721.v1

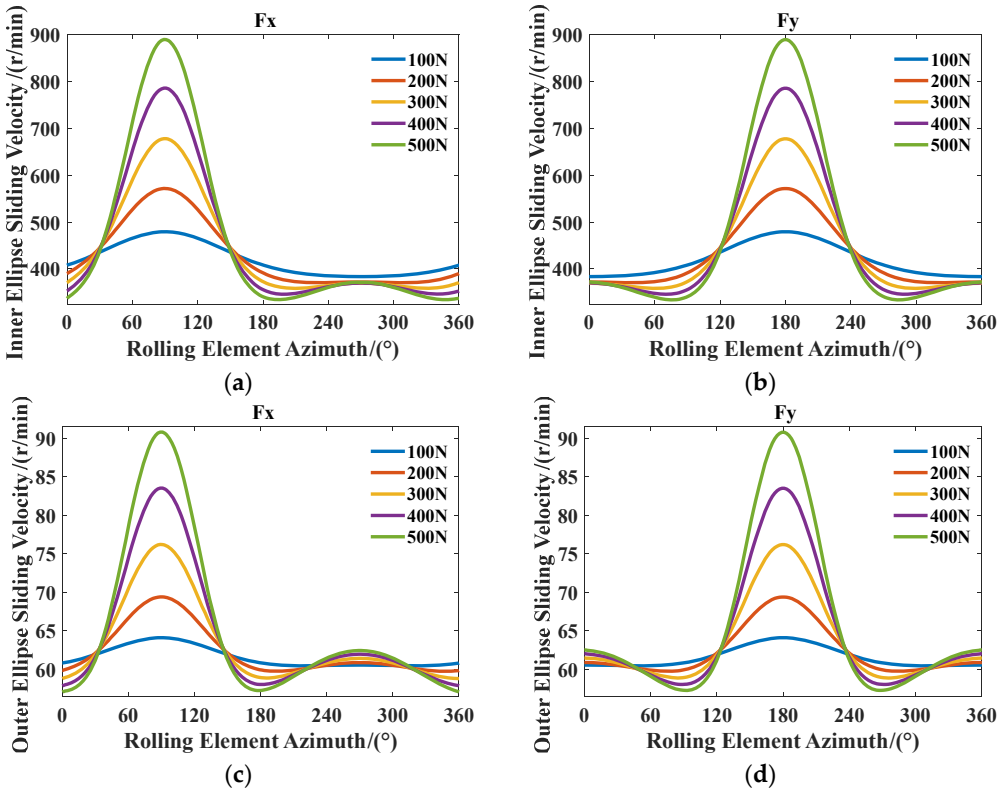

Figure 14. Effect of unilateral radial force on sliding velocity at the center of raceway contact ellipse.

As shown in Figure 14, in the bearing zone, the sliding velocity is positively correlated with the radial force F_x and F_y. In the non-bearing area, sliding velocity presents a W-shaped change law, in which the W-shaped phenomenon of the outer raceways is more obvious than that of the inner raceways, and the W-shaped change is gradually obvious with the increase of radial force.

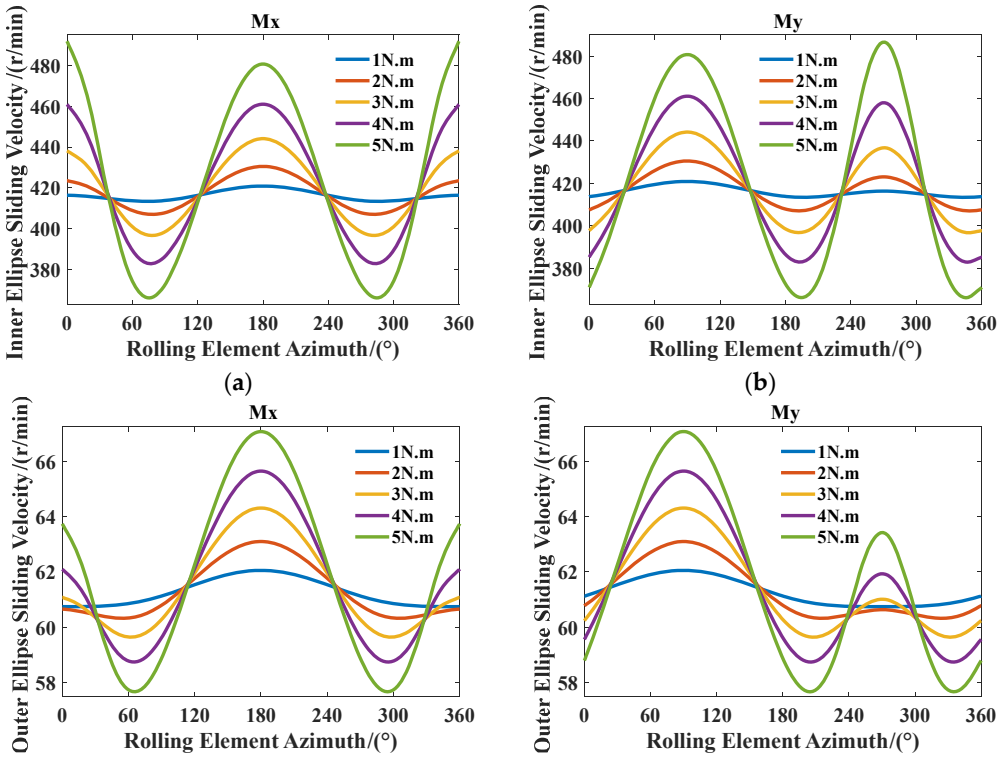

 doi:10.20944/preprints202604.1721.v1

(c) (d)

Figure 15. Effect of unilateral torque on sliding velocity at the center of raceway contact ellipse.

As shown in Figure 15, there are two bearing zones when torque is applied, when M_x acts, the azimuth around 0°and 180°is the bearing zone; when M_y acts, the azimuth around 90°and 270°is the bearing zone. In the bearing zone, sliding velocity is positively correlated with M_x and M_y. In the non-load zone, the inner raceway's sliding velocity is negatively correlated with M_x and M_y, while presents a W-shaped change rule in the outer raceway, and the W-shaped change is gradually obvious with the increase of torque.

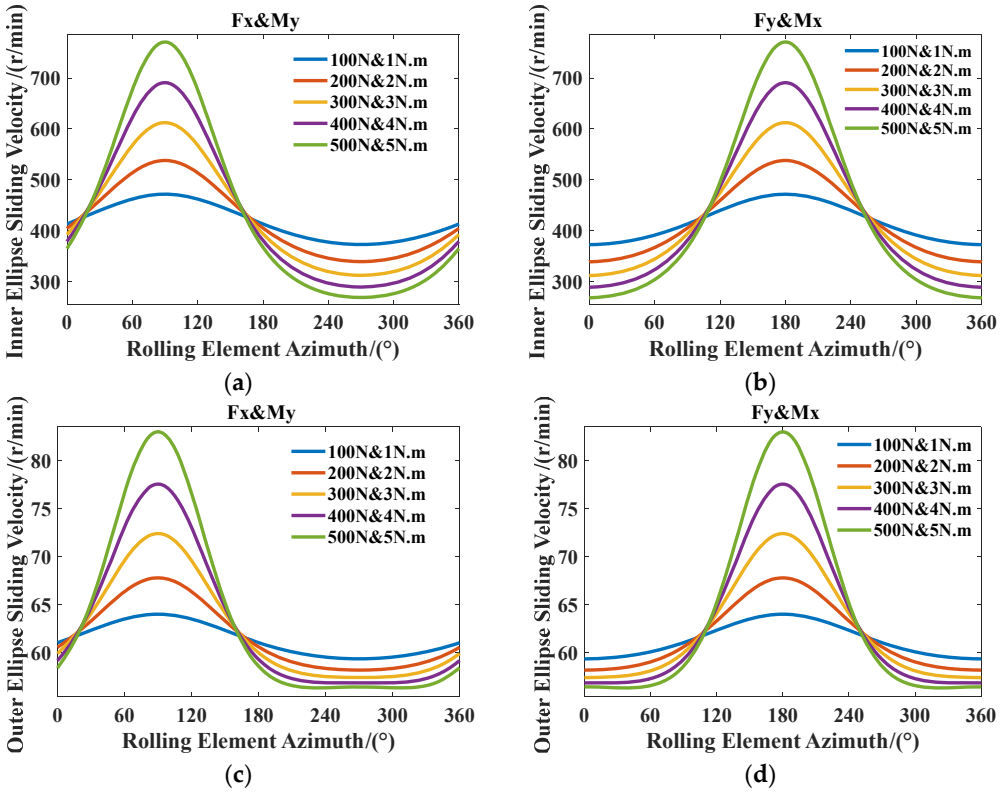

Figure 16. Effect of unilateral radial force and torque on sliding velocity at the center of raceway contact ellipse.

As shown in Figure 16, the positive direction of the torque M_y is the same as the radial force F_x, and M_x, F_y act in the same direction. In the bearing zone, sliding velocity is positively correlated with the combined load. In the non-bearing zone, the sliding velocity is negatively correlated with the combined load.

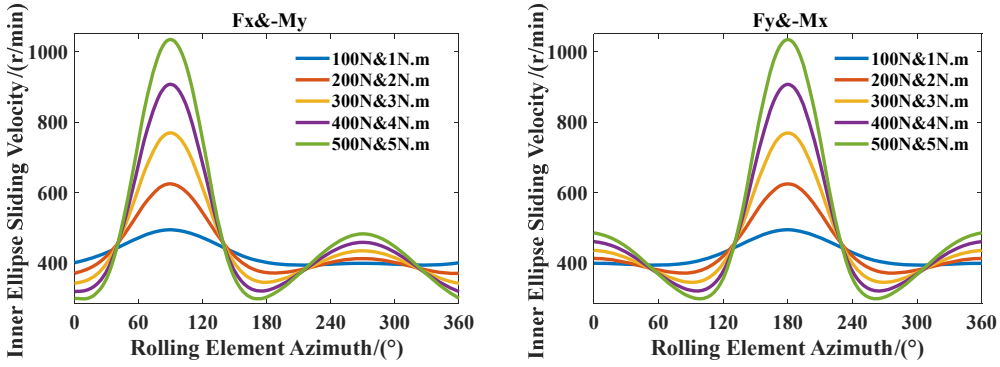

 doi:10.20944/preprints202604.1721.v1

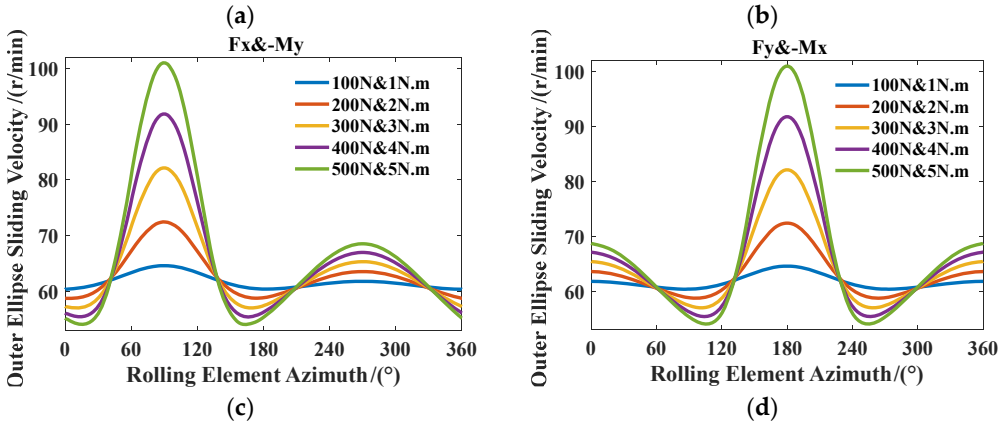

Figure 17. Effect of unilateral radial force and torque on sliding velocity at the center of raceway contact ellipse.

As shown in Figure 17, the positive direction of the torque $-M_y$ is opposite to the radial force F_x, and $-M_x$, F_y act in opposite directions. In the bearing zone, sliding velocity is positively correlated with the combined load, while presents a W-shaped change in the non-load zone, and the W-shaped change is gradually obvious with the increase of the combined load.

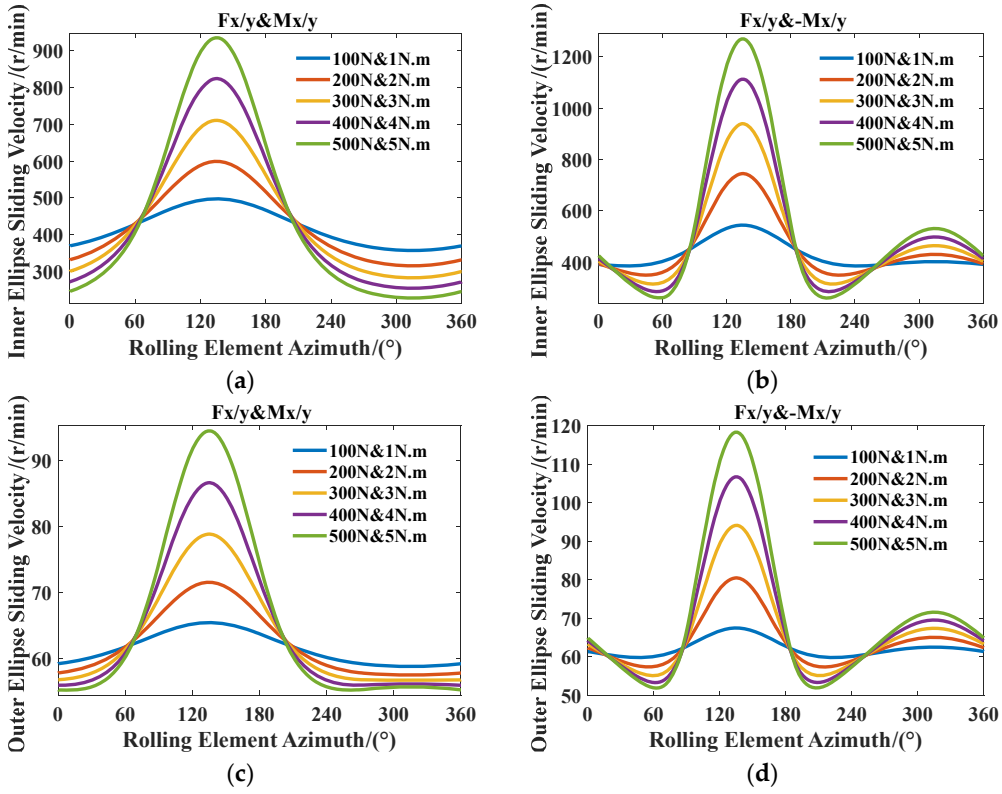

Figure 18. Effect of combined load on sliding velocity at the center of raceway contact ellipse.

As shown in Figure 18, When the radial force and torque are acting in the same direction, sliding velocity is positively correlated with the combined load in the bearing region and negatively correlated with the combined load in the non-bearing region. When the radial force and torque act in the opposite direction, sliding velocity is positively correlated with the combined load in the bearing region, and presents a W-shaped change in the non-bearing region, and the W-shaped change is gradually obvious with the increase of the combined load.

 doi:10.20944/preprints202604.1721.v1

4. Conclusions

In this paper, a five-degree-of-freedom quasi-static model of angular contact ball bearings is established and its accuracy is verified. A modified Archard model is applied to develop wear volume models for the inner and outer raceways. Based on the established models, the nonlinear variation patterns of dynamic parameters related to raceway wear are investigated under rotational speed, single loads, and combined loads.

The dynamic parameters present different change laws in the inner and outer raceway. The centrifugal force enhances the contact between ball and outer raceway, and weakens the contact in the inner raceway. In the bearing zone, the dynamic parameters are positively correlated with single and combined loads, while negatively correlated or show a W-shaped change law in the non-bearing zone, and this unique nonlinear change will gradually become obvious with the increase of the applied load.

Author Contributions: Conceptualization, X.L. and F.S.; methodology, X.L.; software, X.L.; validation, X.L.; formal analysis, X.L.; investigation, C.Z.; resources, F.S. and R.M. and J.L.; data curation, X.L.; writing—original draft preparation, X.L.; writing—review and editing, F.S.; visualization, W.Z.; supervision, J.J.; project administration, F.X.; funding acquisition, F.S. All authors have read and agreed to the published version of the manuscript.

Funding: This research was funded by Liaoning Provincial Science and Technology Major Project (Grant No. 2025JH111700005), Key R&D Project of the Liaoning Provincial Science and Technology Plan Joint Program (Grant No. 2025JH2/101800446), Xingliao Talent Plan (Grant No. XLYC2503136).

Data Availability Statement: The raw data supporting the conclusions of this article will be made available by the authors upon request.

Acknowledgments: In this study, we have received a great deal of valuable support, for which we express our sincere gratitude. Special thanks go to Professor Sun for his administrative and technical support, which has greatly enhanced the efficiency and quality of our research.

Conflicts of Interest: The author(s) declared no potential conflicts of interest with respect to the research, authorship, and/or publication of this article.

References

1. Jones A B. A general theory for elastically constrained ball and radial roller bearings under arbitrary load and speed conditions[J]. Journal of Basic Engineering, 1960, 82(2): 309:320.
2. HARRIS T A. Rolling bearing analysis[M]. New York: John Wiley and Sons, 2001.
3. DE M J M, VREE J M, MAAS D A. Equilibrium and associated load distribution in ball and roller bearings loaded in five degrees of freedom while neglecting friction—part1: general theory and application to ball bearings[J]. Journal of Tribology, 1989, 111(1): 142-148.
4. Jiang S, Mao H. Investigation of variable optimum preload for a machine tool spindle[J]. International Journal of Machine Tools and Manufacture, 2010, 50(1): 19-28.
5. GUO Y, PARKER R G. Stiffness matrix calculation of rolling element bearings using a finite element /contact mechanics model[J]. Mechanism and Machine Theory, 2012, 51: 32-45.
6. GUNDUZ A, SINGH R. Stiffness matrix formulation for double row angular contact ball bearings:Analytical development and validation[J]. Journal of Sound & Vibration, 2013, 332(22): 5898-5916.
7. WANG W Z, HU L, ZHANG S G, et al. Modeling angular contact ball bearing without raceway control hypothesis[J]. Mechanism and Machine Theory, 2014, 82: 154-172.
8. HE P P, GAO F, YAN L, et al. Study on thermo-mechanical coupling characteristics of angle contact ball bearing with fixposition preload[J]. Industrial Lubrication and Tribology, 2019, 71(6): 795-802.
9. LIM T C, SINGH R. Vibration transmission through rolling element bearings, part II: system studies[J]. Journal of Sound & Vibration, 1990, 139(2): 201-225.

 doi:10.20944/preprints202604.1721.v1

10. EL-THALJI I, JANTUNEN E. A descriptive model of wear evolution in rolling bearings[J]. Engineering Failure Analysis, 2014 (45): 204-224.
11. ALFARES M A, EISHARKAWY A A. Effects of axial preloading of angular contact ball bearings on the dynamics of a grinding machine spindle system[J]. Journal of Materials Processing Technology, 2003, 136(1): 48-59.
12. LU J J, QIU M, LI Y C. Probabilistic wear lifetime of hinge configurations resolved on numerical simulation[J]. Journal of Mechanical Engineering, 2015, 51(11): 56-63.
13. Olofsson U, Andersson S, Björklund S. Simulation of mild wear in boundary lubricated spherical roller thrust bearings[J]. Wear, 2000,241(2):180-185.
14. Janakiraman V, Li S, Kahraman A. An Investigation of the Impacts of Contact Parameters on Wear Coefficient[J]. Journal of Tribology, 2014, 136(3): 69-74.
15. Liu C H, Chen X Y, Gu J M, et al. High-speed wear lifetime analysis of instrument ball bearings[J]. Proceedings of the Institution of Mechanical Engineers, Part J: Journal of Engineering Tribology, 2009, 223(3): 497-510.
16. Yang L J. Wear coefficient equation for aluminium based matrix composites against steel disc[J]. Wear, 2003,255(1-6): 579-592.
17. Shen X, Liu Y, Cao L, et al. Numerical Simulation of Sliding Wear for Self-lubricating Spherical Plain Bearings[J]. Journal of Materials Research and Technology, 2012,1(1): 8-12.
18. David, E, Brewe, et al. Simplified Solution for Elliptical-Contact Deformation Between Two Elastic Solids[J]. Journal of Tribology, 1977.
19. WAN Changsen. Analytical method of rolling bearing [M]. Beijing: China Machine Press, 1987.